Chapter 9
Influence of Sensor Uncertainty on Frequency Response Functions of Hydraulic Accumulators

Oscar L. Lefemmine, Manuel Rexer, Maximilian M. G. Kuhr, and Peter F. Pelz

Abstract The determination of the frequency response function (FRF) of hydraulic components, such as hydraulic accumulators, is typically carried out in the frequency domain. However, due to stochastic and systematic measurement errors, the obtained FRF, i.e., the accumulator's frequency-dependent stiffness, is also subject to uncertainty. In particular, the systematic measurement uncertainty of the sensors used, which is typically neglected during uncertainty propagation into the frequency domain, is crucial for determining the uncertainty value of the frequency-dependent stiffness. At the Chair of Fluid Systems, investigations are focused on optimizing the energy density of hydraulic accumulators. Within the scope of this paper, PUR foam is introduced into the gas-side of the accumulator, increasing its thermal capacity. The foam's porous structure, provides a large area for heat transfer, leading to a reduction in stiffness while maintaining the same accumulator geometry. To predict the dynamic behavior, analytical models are set up and compared to experimental measurement data gathered with an one-axis servo-hydraulic test rig, focusing on the pressure response to harmonic volume displacement. In order to validate the analytical models, it is indispensable to determine the uncertainty in measurement data. Therefore, this paper focuses on applying an uncertainty quantification framework, presented previously at IMAC-XLII, to quantify the impact of different types of uncertainty on the measurement results. The framework uses different sensor error models in combination with Monte Carlo simulations to propagate the modeled errors into the frequency domain. This approach is applied to evaluate measurements taken on hydraulic accumulators with PUR foam infill, investigating the influence of uncertainty.

Keywords Uncertainty · Systematic Error · Frequency Domain · Monte Carlo Simulation · Hydraulic accumulators

Introduction

The behavior of dynamic systems is determined by their intrinsic structure, which can be described using spring, damper and mass models and characterized by parameters such as stiffness and damping coefficients. Dynamic systems are found in various forms across many fields. From bridges to powertrains and the periodic detachment of cavitation clouds, understanding the response to external excitation is crucial for the design and operation of these systems. The determination of dynamic behavior is achieved through analytical models, simulations, or experiments. Since experimental investigations are often considered preferable [1, 2], knowledge of the propagation of uncertainty inherently linked to the use of measurement equipment is essential for accurate interpretation of results. A thorough understanding of a dynamic system's behavior enables optimal design and control [3].

Although determining dynamic characteristics in the frequency domain is standard practice, proper quantification of the uncertainty in the identified quantities is often lacking. This is primarily due to the complex propagation of both random and systematic uncertainty from the time domain to the frequency domain, or vice versa. Generally, the Joint Committee for Guides in Metrology (JCGM) [4] distinguishes between two types of uncertainty: type A uncertainty, i.e., normally distributed stochastic uncertainty, and type B uncertainty, i.e., systematic measurement uncertainty with unknown distribution. Extensive literature exists on the propagation of type A uncertainty into the frequency domain [5–9]. In contrast, for type B uncertainty, only conservative assumptions are typically made, as investigated by Kuhr [10]. According to JCGM, type A uncertainty is handled using Gaussian uncertainty propagation, whereas type B uncertainty require more sophisticated approaches, such as Monte Carlo simulations [4].

Oscar L. Lefemmine · Manuel Rexer · Maximilian M. G. Kuhr · Peter F. Pelz
Chair of Fluid Systems, Technische Universität Darmstadt, 64287 Darmstadt, Germany
e-mail: oscar.lefemmine@tu-darmstadt.de; manuel.rexer@tu-darmstadt.de; maximilian.kuhr@tu-darmstadt.de; peter.pelz@tu-darmstadt.de

Roland Platz et al. (eds.), *Model Validation and Uncertainty Quantification, Vol. 3*, Conference Proceedings of the Society for Experimental Mechanics Series, https://doi.org/10.13052/97887-438-0148-1_9

Rexer et al. [11] used Monte Carlo simulations in their investigations to determine simple propagation laws of sensor uncertainty into the frequency domain and, thus, the influence on the magnitude and phase of complex Fourier coefficients. In this paper, the influence of systematic sensor errors on the frequency-dependent stiffness of hydraulic accumulators is investigated by applying the propagation laws found by Rexer et al. [11]. First, some background information on the propagation modeling will be provided. In addition to that, some basics on the frequency-dependent stiffness of gas volumes will be described, with particular focus on the physical effects occurring at different frequencies. To present the experimental procedure, the test rig and the experimental setup are explained in more detail. In conclusion, the results of the error propagation will be presented and discussed.

Uncertainty propagation into frequency domain

To characterize the response of hydraulic accumulators to harmonic excitation, pressure and temperature measurements within the accumulator are used to determine its frequency-dependent stiffness. Following the approach outlined by Puff [12] and Hedrich et al. [13, 14], these signals are transformed into the frequency domain using Fast Fourier Transforms (FFT), allowing the evaluation of the accumulator's stiffness across different excitation frequencies.

The following description of error propagation is based on the methods of Rexer et al. [11]. The use of sensors is directly associated with inaccuracies in the recorded measurements. The transfer behavior cannot be considered ideal, so a sensor error $E_i = y_i - x_i$ is to be expected between the measured value y_i and the actual value x_i. While this kind of error represents a specific deviation, unknown measurement errors can be treated statistically using probability distributions. This approach enables the quantification of uncertainty, offering a framework for analysis through statistical methods. In other words, the uncertainty δ_i of the measured value y_i defines an interval around the mean value $\bar{y}$ within which the true value is likely to fall. Hence, $y_i = \bar{y}_i \pm \delta_{95}(y_i)$ with a confidence interval for δ_i of 95 %.

Generally, sensor errors can be divided into random errors and systematic errors, with the latter further classified into bias or offset, sensitivity, linearity, and hysteresis errors [15], cf. fig. 1. Data sheets provided by manufacturers often address often address errors by providing deviation bounds, δ_{lin} and δ_{hys}, as shown in fig. 1, within which the measured value is expected to fall. However, the distribution is unknown and can therefore be described as incertitude according to Pelz et al. [3]. To utilize Monte Carlo simulations, generalized sensor and error models are required. Typically, sensor transfer behavior is approximated using an ideal characteristic curve y as a function of the input signal x, with slope s and offset o. To account for the four types of sensor errors, additional terms $\mathrm{fn}(\mathrm{x}, \dot{\mathrm{x}})$ are introduced. It is assumed that linearity errors vary with the input signal, thus $E_{\mathrm{lin}} = \mathrm{fn}(\mathrm{x})$, and that hysteresis errors depend on both the input signal and the direction from which the value is approached, hence $E_{\mathrm{hys}} = \mathrm{fn}(\mathrm{x}, \dot{\mathrm{x}})$. The sensor model can then be described with

$$y = sx + o + E_{\mathrm{bias}} + E_{\mathrm{s}}x + E_{\mathrm{lin}}(x) + E_{\mathrm{hys}}(x, \dot{x}). \tag{1}$$

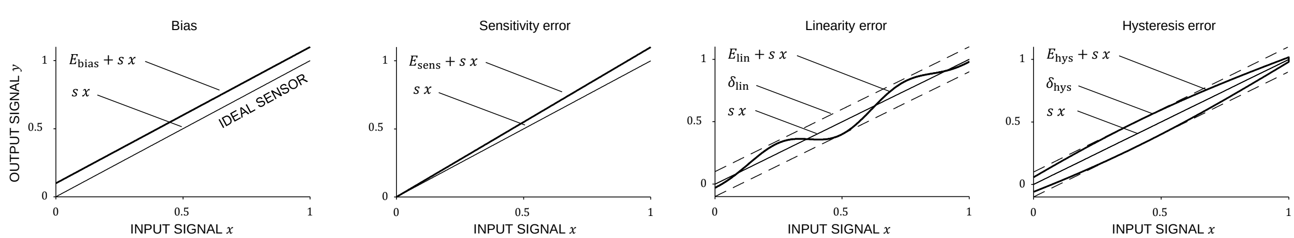

Fig. 1 Different types of sensor errors described in [15]. Offset errors result in a static deviation in the output signal and should be differentiated from sensor offsets defined by their measuring range. Sensitivity errors show a deviation from the sensor's ideal slope. Linearity errors and hysteresis errors can take various, complex forms [11].

Bias and sensitivity errors can be easily modeled using constant values E_{bias} and E_{s}. In the latter case, E_{s} represents the slope of the faulty characteristic curve. The values of these constants, without the corresponding probability function, are typically provided in the sensor's data sheet. To propagate uncertainty effectively rather than just performing interval estimation, the JCGM suggests assuming a uniform distribution as a conservative estimate [4]. Both uncertainties can be directly propagated into the frequency domain

$$\tilde{\delta}_{\text{bias}}(|Y(\omega)|) = \begin{cases} \delta_{\text{bias}}, & \omega = 0 \\ 0, \ \forall & \omega \neq 0 \end{cases}, \tag{2}$$

$$\tilde{\delta}_{\text{s}}(|Y(\omega)|) = \delta_{\text{s}}. \tag{3}$$

Regarding linearity and hysteresis errors, modeling their behavior is more complex. To describe the influence on a measured signal, Rexer et al. [11] follow an approach based on Fourier transformation, where an arbitrary signal can be broken down into a series of harmonic signals. Hence, to describe linearity errors in eq. (4), a sum of M sinusoidal signals is used

$$E_{\text{lin}}(x) = \sum_i a_i \sin(w_i x + \varphi_i), \quad i = 1...M \in \mathbb{N}_0. \tag{4}$$

In this case, the parameters a_i, w_i, and φ_i, i.e., amplitude, frequency, and phase shift respectively, are considered statistically distributed quantities, cf. table 1. In order to restrict values calculated with eq. (4) within the given sensor bounds stated in the manufacture's data sheet, the equation is scaled with

$$\max[E_{\text{lin}}(x)] \leq \delta_{\text{lin}}. \tag{5}$$

Hysteresis errors are modeled in a similar way. In the case of sensors, hysteresis describes the effect of different measured values depending on the direction of approach. This is taken into account by including the change of the measured signal over time, $\dot{x}$, and approximating the signum function with the hyperbolic tangent function. Analogous to linearity errors, a sum of harmonic signals is used to describe hysteresis errors

$$E_{\text{hys}}(x, \dot{x}) = \sum_i \tanh(\dot{x})\, a_i \sin(w_i x + \varphi_i), \quad i = 1, \dots, M \in \mathbb{N}_0. \tag{6}$$

Table 1 Values used to parametrize the error model given by eq. (4) and eq. (6), as well as the test signal, eq. (8), for the Monte Carlo simulation.

	Parameter	Value	Distribution
Amplitude (error)	a_i	$U[0, 1]$	uniform
Phase shift (error)	φ_i	$U[0, 2\pi]$	uniform
Wavelength	ω_i	$\lvert N(0, \sigma)\rvert$	half-normal
Sample frequency	f_{sample}	1 kHz	-
Duration	L	1 s	-
Signal frequency	Ω	10 Hz	-
Offset	o	10	-
Amplitude (test signal)	$\hat{a}$	1	-
Phase shift (test signal)	Φ	45°	-

For preliminary investigations, the distribution of the parameters a_i, w_i, and φ_i was set up according to table 1. Different Monte Carlo simulations for the linearity error E_{lin} showed that a uniform distribution could not be realized by changing the parameters a_i, w_i, and φ_i, or the values of their respective distributions. fig. 2 illustrates how the distribution changes, for example, from an arcsine distribution to a normal distribution when the standard deviation of the wavelength w_i is varied. Hence, the assumptions according to JCGM cannot be met. To generate a uniform distribution of the linearity error E_{lin}, Rexer et al. [11] adopt the approach of describing the amplitude a_i as a function of the wavelength w_i in the form of

$$a_i = \frac{1}{w_i^2}. \tag{7}$$

Performing Monte Carlo simulations using the modification in eq. (7) led to a uniform distribution of the linearity error, cf. fig. 3.

To investigate the influence of sensor errors on the frequency response, a test signal must be generated. Hence, a generic harmonic input signal is used to feed the sensor model

$$x = o + \hat{a} \sin(2\pi\Omega t + \phi). \tag{8}$$

In eq. (8), o is an offset, $\hat{a}$ the signal amplitude, Ω the excitation frequency, and ϕ a phase shift. Both models, i.e., eq. (1) and eq. (8), are used in a Monte Carlo simulation to investigate the influence on the magnitude and phase of the frequency response. For this, the test signal is characterized according to table 1.

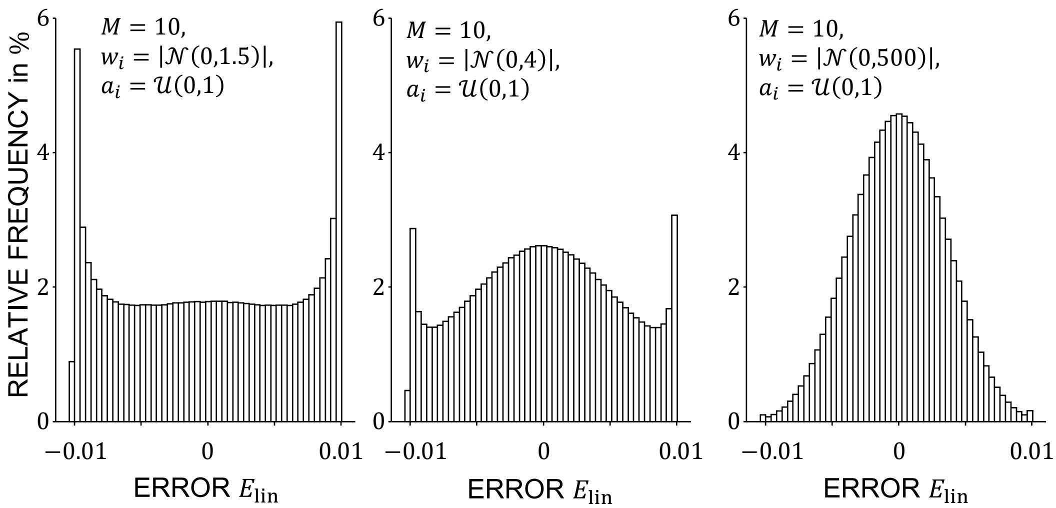

Fig. 2 Distribution of linearity error resulting from the Monte Carlo simulation using parameters in table 1 [11]. The figure shows that the distribution changes from an arcsine distribution to a normal distribution as the standard deviation of the uniform distribution of the wavelength w_i increases. The arcsine distribution results from a harmonic sinusoidal function being sampled with equidistant time steps.

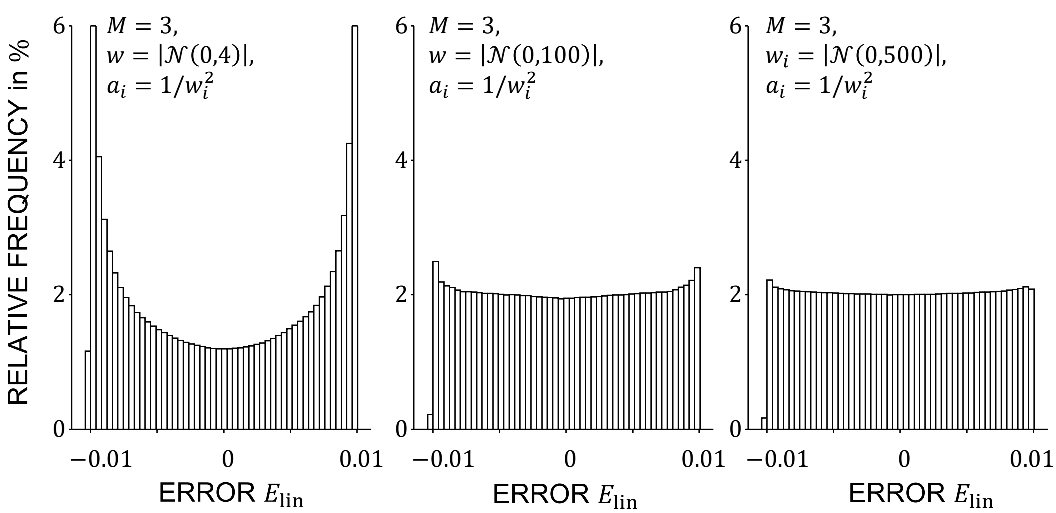

Fig. 3 Resulting distribution using parameters in table 1 and eq. (7) [11]. The distribution changes from an arcsine distribution to a uniform shape. Hence, the JCGM's suggestion of assuming a uniform distribution as a conservative estimation is met.

After having modeled the sensor characteristic and the test signal, a final Monte Carlo simulation demonstrates the influence on the magnitude and phase of the frequency response function. To achieve this, errors are generated randomly, and the resulting output signal y is then Fourier-transformed. A total of 10^6 iterations are performed to obtain the results shown in fig. 4. The cross-shaped form of the scatter plot indicates that the linearity and hysteresis errors are independent of each other in the frequency domain. A sensitivity analysis varying the sensor error bounds δ_{lin} and δ_{hys} reveals the linear dependency of the systematic error for both magnitude and phase on δ_{lin} and δ_{hys}, respectively. From fig. 5, two propagation laws can be deduced:

$$\tilde{\delta}_{\mathrm{lin}}(|Y(\Omega)|) = 0.263\,\delta_{\mathrm{lin}}(y), \tag{9}$$

$$\tilde{\delta}_{\mathrm{hys}}(\angle[Y(\Omega)]) = \tan^{-1}\left(\frac{0.235\,\delta_{\mathrm{hys}}(y)}{|Y(\Omega)|}\right). \tag{10}$$

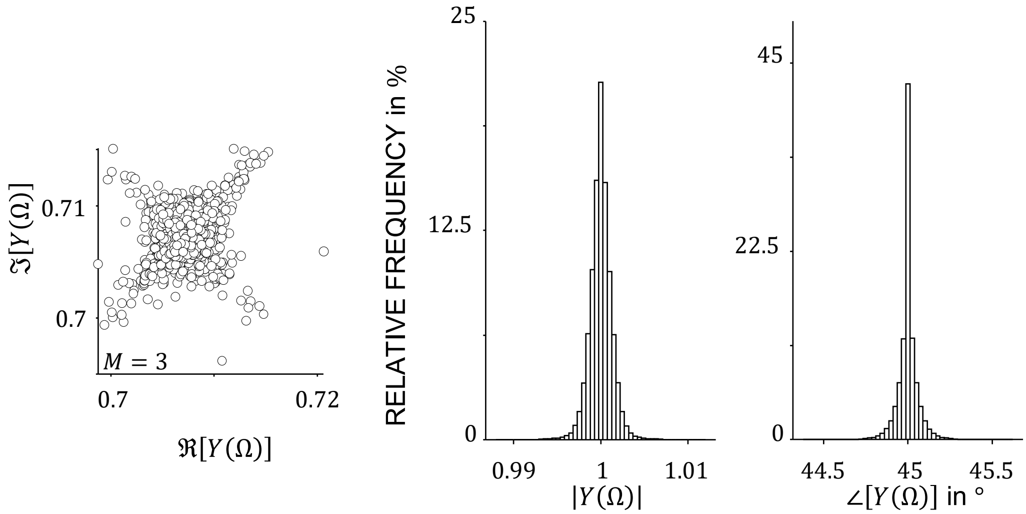

Fig. 4 Results of the Monte Carlo simulation with the final determined parameters [11].

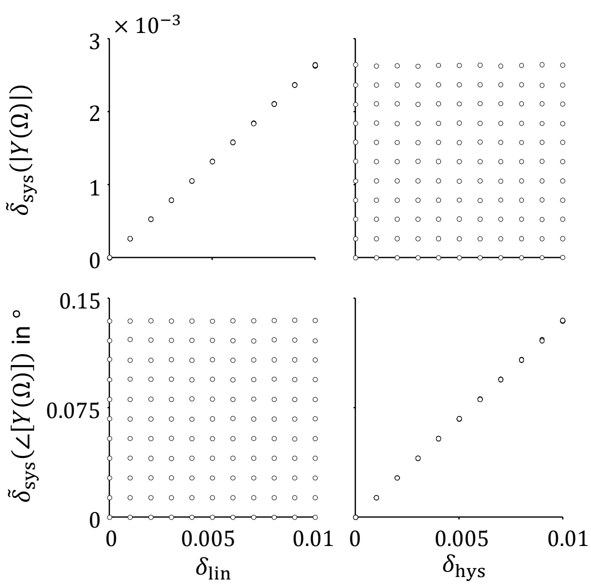

Fig. 5 Influence of the uncertainty intervals of the linearity and hysteresis errors on the standard deviation of magnitude and phase of the Fourier coefficient $Y(\Omega)$ [11].

After modeling sensor errors such as bias, sensitivity, linearity, and hysteresis, and simulating their propagation into the frequency domain using Monte Carlo simulations, the influence on the measurement process can be quantified. The methodology demonstrated how systematic errors affect both the magnitude and phase of frequency response functions and showed a linear dependency on their respective uncertainty bounds. With this groundwork laid, basic knowledge about the frequency-dependent stiffness of hydraulic accumulators is given.

Frequency-dependent stiffness of hydraulic accumulators

Hydraulic accumulators function as conservative spring elements within hydraulic systems. Commercial vehicles like tractors, wheel loaders, and dump trucks often utilize compressed gas for suspension. Since hydraulic oil systems are commonly integrated into these vehicles, hydro-pneumatic suspensions can be implemented. In spring-mass systems, lower spring stiffness results in better vibration isolation. However, stiffness decreases as the volume of the hydraulic accumulator increases [16, 17]. Components for vehicle suspensions must be small and light due to space constraints and the need to minimize weight, which affects energy consumption for propulsion. The integration of porous materials offers an effective approach to increasing the thermal capacity of hydraulic accumulators, enabling a reduction in size without compromising stiffness. In diaphragm accumulators, pressure is applied to the oil side of a flexible diaphragm, compressing the gas, typically nitrogen, on the other side. Figure 6 illustrates the interior of an accumulator with foam infill.

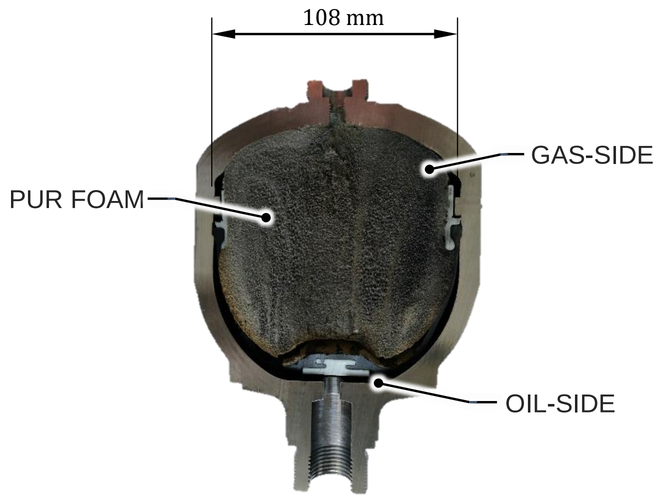

Fig. 6 Cross-sectional view of a hydraulic accumulator with PUR foam infill.

Accumulators are typically prefilled with a gas to a specified precharge pressure p_0, occupying an initial volume V_0. They are subsequently pressurized with hydraulic fluid to the operating pressure p_1 and then subjected to oscillatory volume changes at an angular frequency Ω, leading to time-dependent pressure p and volume V. These parameters form the basis for describing the dynamic stiffness of the gas volume. The dynamic behavior of gas volumes changes depending on the excitation frequency, resulting in increased stiffness as the frequency rises. Pelz and Buttenbender [17] provide a foundational model for the frequency-dependent stiffness. While their model does not account for the influence of porous materials, studies by Hartig [16], Rexer [18], Rexer et al. [19], and Pelz et al. [20] provide insights into the interactions between gas and foams, activated carbon, and other porous materials in both air springs and hydraulic accumulators. An increase in stiffness is observed as the state change transitions from isothermal at low excitation frequencies to adiabatic at high frequencies. Hartig [16] and Rexer [18] identify different plateaus in their stiffness models, which are attributed to changing interactions between gas and infill material.

The frequency-dependent stiffness K is defined as the change in pressure $\mathrm{d}p$ with respect to a periodically applied volumetric displacement $\mathrm{d}V$. In order to enable a meaningful comparison between different types of hydraulic accumulators, it is useful to non-dimensionalize the stiffness K. For this purpose, the pressure p_1 and the corresponding volume V_1 of the accumulator are used. Introducing the dimensionless variables $p = p^+ p_1$ and $V = V^+ V_1$, the dimensionless stiffness is defined as:

$$K^+ = \frac{p^+}{V^+}. \tag{11}$$

The frequency is non-dimensionalized in a similar manner, using a characteristic length L, thermal conductivity λ, gas density ϱ, and specific heat capacity at constant pressure c_p. The resulting dimensionless frequency corresponds to the Péclet number:

$$Pe = \frac{\Omega L^2}{\lambda/(\varrho c_\mathrm{p})}. \tag{12}$$

Experimental setup

For the experimental evaluation of the frequency-dependent stiffness, a HYDAC hydraulic accumulator (SBO450E-0.6A6-112U-450AK) with a nominal volume of 600 ml is utilized. Prior to integrating the accumulator into the test rig, pieces of PUR foam with two different porosities, measured in pores per inch (PPI), were shaped to fit the accumulator's contours and then inserted into the gas-side chamber. Nitrogen was then charged into the accumulator up to 40 bar. Before starting the harmonic excitation, an operating pressure of 60 bar was applied to the oil-side chamber via an external hydraulic system. The test rig features a temperature-controlled measurement chamber, enabling the setting of the ambient temperature, cf. fig. 7. The experiment started once thermal equilibrium was achieved, with the gas temperature matching the set ambient temperature. A sinusoidal excitation with parameters given in table 2 was applied to the accumulator, and the pressure response was measured at various frequencies. The measurement data is available on the European database Zenodo [21–24].

Table 2 Parameters used for the excitation signal of the test rig. The cylinder of the one-axis servo-hydraulic test rig performs a harmonic sinusoidal motion, resulting in a volumetric displacement of the oil in the accumulator. Hydraulic accumulators are typically prefilled with nitrogen and pressurized to the operating pressure.

	Value
Amplitude	2 mm
Frequency	$0.1 - 20$ Hz
Prepressure N_2	40 bar
Operating Pressure	60 bar

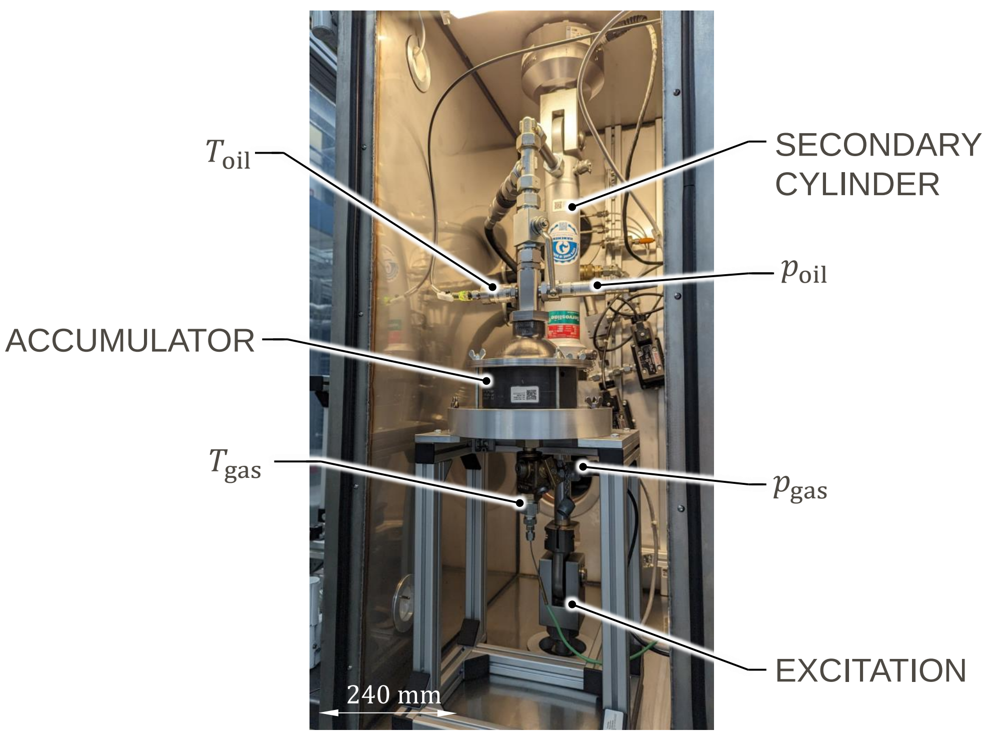

Fig. 7 Image of the hydraulic accumulator under investigation, installed in the test rig. The cylinder of the one-axis servo-hydraulic test rig moves a secondary cylinder that causes the displacement of a defined volume of oil. The entire assembly is situated in a temperature-controlled chamber that is connected to an external climatic chamber.

Results and discussion

For the evaluation of the accumulator's stiffness, a MATLAB based software framework for calculating uncertainty in the frequency domain is used [25]. The measured sensor signals for pressure and cylinder displacement are subject to sensor errors. Consequently, calculated values, such as the dimensionless stiffness, are also subject to uncertainty, where these uncertainties propagate into the frequency domain. The uncertainties considered are calculated according to eq. (13) and eq. (14).

$$\tilde{\delta}_{\text{sys}}(|Y(\Omega)|) = \begin{cases} \tilde{\delta}_{\text{bias}} + \tilde{\delta}_{\text{sens}} + \tilde{\delta}_{\text{lin}}, & \Omega = 0 \\ \tilde{\delta}_{\text{sens}} + \tilde{\delta}_{\text{lin}}, \forall & \Omega \neq 0 \end{cases} \quad , \tag{13}$$

$$\tilde{\delta}_{\text{sys}}(\angle[Y(\Omega)]) = \begin{cases} 0, & \Omega = 0 \\ \tilde{\delta}_{\text{hys}}, \forall & \Omega \neq 0 \end{cases} \quad . \tag{14}$$

The results in fig. 8 show the dimensionless stiffness of an empty hydraulic accumulator with a nominal capacity of 600 ml, as well as with three types of porous materials. The upper blue data points correspond to an accumulator without infill. It can be seen that introducing a porous material into the accumulator significantly changes its properties. With increasing porosity, the surface area of the foam increases, resulting in more heat being transferred to the foam.

At a certain frequency, the stiffness with a 60 PPI foam exceeds that of the 40 PPI foam. This behavior is unexpected and requires further investigation. The data points for the 80 PPI foam show the most favorable results in terms of reducing the stiffness of the hydraulic accumulator. The results demonstrate that a reduction in stiffness can be achieved without changing the accumulator's size. According to Hartig [16], a plateau in the mid-frequency range can be observed before the stiffness increases at higher frequencies. At lower frequencies, the state change can be described as isothermal, with heat being transferred to the ambient environment through the accumulator wall. As the frequency increases beyond a certain threshold, the state change becomes adiabatic, and heat exchange occurs only between the gas and the foam via the large surface area of the porous material.

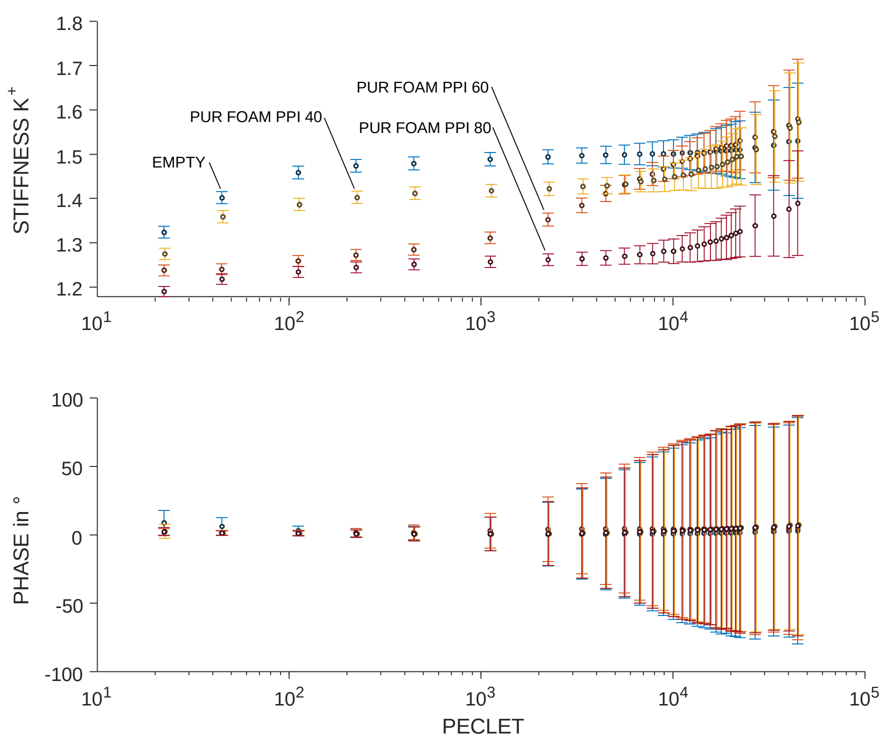

Fig. 8 Results from the measurement and evaluation of the dimensionless stiffness are presented. The error bars are calculated according to eq. (13) and eq. (14) for the magnitude and phase, respectively. For both porosities of 60 PPI and 80 PPI, the stiffness shows a similar shape.

Acknowledgments This work was funded by the Deutsche Forschungsgemeinschaft (DFG, German Research Foundation) — Project number 57157498—SFB805.

References

1. Isermann, R. *Mechatronic Systems: Fundamentals*. Springer London, London (2005).
2. Pintelon, R. and Schoukens, J. *System Identification: A Frequency Domain Approach*. John Wiley & Sons, New York, NY, 2., auflage edition (2012).
3. Pelz, P., Groche, P., Pfetsch, M.E., and Schäffner, M.F. *Mastering Uncertainty in Mechanical Engineering*. Universitäts- und Landesbibliothek, Darmstadt (2023).
4. BIPM, IEC, IFCC, ILAC, ISO, IUPAC, IUPAP, and OIML. *Evaluation of measurement data — Guide to the expression of uncertainty in measurement* (2008).
5. Betta, G., Liguori, C., and Pietrosanto, A. "Propagation of uncertainty in a discrete fourier transform algorithm". *Measurement*, 27(4):231–239 (2000).
6. Medina, L., Ruiz, R., and Diaz, S. "A simple approach to determine uncertainty bounds on bearing rotordynamic coefficients identification". In *Volume 5: Structures and Dynamics, Parts A and B*, pages 1279–1287. ASMEDC (2008).
7. Llatas, I., Medina U., L., and Diaz, S. "Measurement uncertainty propagation in parameter identification of mechanical systems in frequency domain" (2010).
8. Alex Moreland, J., Childs, D.W., and Bullock, J.T. "Measured static and rotordynamic characteristics of a smooth-stator/grooved-rotor liquid annular seal". *Journal of Fluids Engineering*, 140(10) (2018).
9. Eichstädt, S. and Wilkens, V. "Gum2dft—a software tool for uncertainty evaluation of transient signals in the frequency domain". *Measurement Science and Technology*, 27(5):055001 (2016).
10. Kuhr, M. "Identification of the dynamic force and moment characteristics of annular gaps using linear independent rotor whirling motions". *Mechanical Systems and Signal Processing*, 187:109936 (2023).
11. Rexer, M., Pelz, P.F., and Kuhr, M.M. *Uncertainty Propagation of Systematic Sensor Errors into the Frequency Domain* (2023).
12. Puff, M. *Entwicklung einer Prüfspezifikation zur Charakterisierung von Luftfedern*, volume 223 of *FAT-Schriftenreihe*. VDA, Berlin (2009).
13. Hedrich, P., Lenz, E., Brötz, N., and Pelz, P. *Active Pneumatic Suspension for Future Autonomous Vehicles: Design, Prove of Concept and Hardware-in-the-Loop Simulations*. Universitätsbibliothek der RWTH Aachen, Aachen (2018).
14. Hedrich, P. "Minimizing of kinetosis during autonomous driving". *ATZ worldwide*, 120(7-8):68–75 (2018).
15. Tränkler, H.R. and Fischerauer, G. *Das Ingenieurwissen: Messtechnik*. Springer Berlin Heidelberg, Berlin, Heidelberg (2014).
16. Hartig, J. *Hydrospeicher mit Adsorbentien*. Dissertation, Shaker Verlag.
17. Pelz, P. and Buttenbender, J. *The dynamic stiffness of an air-spring*. Universitäts- und Landesbibliothek, Darmstadt (2022).
18. Rexer, M. *Modellierung und experimentelle Untersuchung eines hydropneumatischen Federbeins mit Schaumspeicher*. Master-thesis, Technische Universität Darmstadt, Darmstadt (2018).
19. Rexer, M., Kloft, P., Bauer, F., Hartig, J., and Pelz, P.F. "Foam accumulators: packaging and weight reduction for mobile applications". In *Volume 1 - Symposium*, pages 181–188. Technische Universität Dresden (12.-14.10.2020).
20. Pelz, P., Groß, T.F., and Schänzle, C. *Hydrospeicher mit Sorbentien - Verhalten, Modellierung und Diskussion*. Universitäts- und Landesbibliothek, Darmstadt (2022).
21. Lefemmine, O., "hydraulic accumulator 600ml purfoamppi40 p0 40bar p1 60bar 20degreecelsius". Zenodo (2024).
22. Lefemmine, O., "hydraulic accumulator 600ml purfoamppi80 p0 40bar p1 60bar 20degreecelsius". Zenodo (2024).
23. Lefemmine, O., "hydraulic accumulator 600ml purfoamppi60 p0 40bar p1 60bar 20degreecelsius". Zenodo (2024).
24. Lefemmine, O., "accumulator 600ml empty p0 40bar p1 60bar". Zenodo (2024).
25. Rexer, M., "Evaluation of heattransfer of gasaccumulators - matlab software to calculate complex nusselt number in frequency domain". Zenodo (2024).